




The Capacity of *Mycobacterium tuberculosis* To Survive Iron Starvation Might Enable It To Persist in Iron-Deprived Microenvironments of Human Granulomas

Krishna Kurthkoti,^{a,*} Hamel Amin,^a Mohlopheni J. Marakalala,^{b,c} Saleena Ghanny,^d  Selvakumar Subbian,^a Alexandra Sakatos,^b Jonathan Livny,^e Sarah M. Fortune,^b Michael Berney,^f G. Marcela Rodriguez^a

Public Health Research Institute at New Jersey Medical School, Rutgers, The State University of New Jersey, Newark, New Jersey, USA^a; Department of Immunology and Infectious Diseases, Harvard T. H. Chan School of Public Health, Boston, Massachusetts, USA^b; Division of Immunology, The Institute of Infectious Disease and Molecular Medicine, University of Cape Town, Observatory, South Africa^c; The Genomics Center at New Jersey Medical School, Rutgers, The State University of New Jersey, Newark, New Jersey, USA^d; The Broad Institute, Cambridge, Massachusetts, USA^e; Department of Microbiology and Immunology, Albert Einstein College of Medicine, Bronx, New York, USA^f

ABSTRACT This study was conducted to investigate the role of iron deprivation in the persistence of *Mycobacterium tuberculosis*. We present evidence of iron restriction in human necrotic granulomas and demonstrate that under iron starvation *M. tuberculosis* persists, refractive to antibiotics and capable of restarting replication when iron is made available. Transcriptomics and metabolomic analyses indicated that the persistence of *M. tuberculosis* under iron starvation is dependent on strict control of endogenous Fe utilization and is associated with upregulation of pathogenicity and intrinsic antibiotic resistance determinants. *M. tuberculosis* mutants compromised in their ability to survive Fe starvation were identified. The findings of this study advance the understanding of the physiological settings that may underpin the chronicity of human tuberculosis (TB) and are relevant to the design of effective antitubercular therapies.

IMPORTANCE One-third of the world population may harbor persistent *M. tuberculosis*, causing an asymptomatic infection that is refractory to treatment and can reactivate to become potentially lethal tuberculosis disease. However, little is known about the factors that trigger and maintain *M. tuberculosis* persistence in infected individuals. Iron is an essential nutrient for *M. tuberculosis* growth. In this study, we show, first, that in human granulomas the immune defense creates microenvironments in which *M. tuberculosis* likely experiences drastic Fe deprivation and, second, that Fe-starved *M. tuberculosis* is capable of long-term persistence without growth. Together, these observations suggest that Fe deprivation in the lung might trigger a state of persistence in *M. tuberculosis* and promote chronic TB. We also identified vulnerabilities of iron-restricted persistent *M. tuberculosis*, which can be exploited for the design of new antitubercular therapies.

KEYWORDS *Mycobacterium tuberculosis*, TB granuloma, iron acquisition, iron deprivation, iron sequestration, latent TB, nutritional immunity, persistence

Mycobacterium tuberculosis is a facultative intracellular pathogen able to survive in an infected host for decades, with little or no replication, undetectable by current diagnostic methods and causing no symptoms but capable of resuming growth and producing active tuberculosis (TB) when immune control weakens (1). This capacity of *M. tuberculosis* to persist in the host is a major obstacle to TB eradication because most

Received 22 June 2017 Accepted 3 July 2017 Published 15 August 2017

Citation Kurthkoti K, Amin H, Marakalala MJ, Ghanny S, Subbian S, Sakatos A, Livny J, Fortune SM, Berney M, Rodriguez GM. 2017. The capacity of *Mycobacterium tuberculosis* to survive iron starvation might enable it to persist in iron-deprived microenvironments of human granulomas. mBio 8:e01092-17. <https://doi.org/10.1128/mBio.01092-17>.

Editor Christina L. Stallings, Washington University in St. Louis School of Medicine

Copyright © 2017 Kurthkoti et al. This is an open-access article distributed under the terms of the [Creative Commons Attribution 4.0 International license](https://creativecommons.org/licenses/by/4.0/).

Address correspondence to G. Marcela Rodriguez, rodrigg2@njms.rutgers.edu.

* Present address: Krishna Kurthkoti, Department of Microbiology and Cell Biology, Indian Institute of Science, Bangalore, India. K.K. and H.A. contributed equally to this work.

antibiotics are inefficient at killing quiescent bacteria (2). The risk of reactivation of latent TB infection (LTBI) to active disease is estimated to be 5 to 10% over a lifetime (3); thus, the approximately 2 billion people predicted to have LTBI constitute an enormous reservoir of new TB cases (3). However, the host conditions that trigger quiescence, the physiology of nonreplicating bacteria, the molecular mechanisms underpinning persistence, and the pathways to reactivation of once-dormant bacilli are not well understood (4).

Like most living organisms, *M. tuberculosis* requires iron (Fe) as a redox cofactor for vital enzymes (4). However, free Fe is not available *in vivo*, and restricting pathogen access to Fe through enhanced production of Fe sequestration proteins and Fe withdrawal from circulation is a major component of the host immune defense, also known as nutritional immunity (5). To compete with the host for Fe, *M. tuberculosis* synthesizes molecules responsible for Fe binding (i.e., siderophores), heme binding, Fe transport, and Fe storage (4). There is ample evidence implicating Fe availability in TB pathogenesis. First, *M. tuberculosis* factors responsible for maintaining Fe homeostasis have been shown to be required for virulence (6–10). Second, several studies have reported that altered host Fe status is linked with TB pathogenesis (11). For instance, high macrophage Fe stores and nutritional Fe overload are associated with increased risk of developing TB and with disease exacerbation (11–13). Thus, an increase in Fe available to *M. tuberculosis* is directly linked to bacterial proliferation and acute TB. In addition, reactivation of LTBI in humans upon Fe supplementation to treat anemia, first reported more than a century ago (14, 15), suggests that Fe deficiency might sustain chronic TB infection, at least in a subset of infected individuals. Nevertheless, the relationship between the *M. tuberculosis* response to Fe deprivation and chronic TB has not been investigated.

In this study, we demonstrate that *M. tuberculosis* has the capacity to persist without growth, under conditions of strict Fe restriction such as those implemented by the human immune defense in necrotic granulomas. Employing genetic, genomic, and metabolomic approaches, we characterized the response of *M. tuberculosis* to prolonged Fe starvation and identified determinants of survival. These results expose a potential role of nutritional immunity in promoting chronic TB and provide a new view of persistent tuberculous bacilli that can provide opportunities for new host- and pathogen-directed therapeutics.

RESULTS

The Fe environment of human granulomas. The pathological hallmark and main stage of human TB infection is the granuloma, an inflammatory lesion that progresses from aggregates of innate immune cells to an organized structure in which the macrophage-rich center is surrounded by a lymphocytic cuff composed of T and B cells (16). As the infection progresses, some granulomas accumulate necrotic material with consequent formation of a caseum at the center, which may undergo liquefaction, sometimes resulting in the formation of a cavity (Fig. 1) (17). Granulomas evolve independently of each other, and different compartments within single granulomas exhibit molecular heterogeneity (18, 19). Therefore, to examine the Fe environment of human granulomas, we analyzed a published data set (19) for the relative abundance of host Fe-sequestering proteins, as indicators of Fe bioavailability in histologically distinct compartments of granulomas, which were separated by laser-guided microdissection and assayed by quantitative mass spectrometry (MS) (19) (Fig. 1). The relative abundance of proteins was based on quantification of a protein in a given dissected histological region compared to all other samples subjected to proteomics. These analyses showed that CD163, the cell surface receptor that mediates internalization of hemoglobin (Hb) (20); heme binding proteins (HEBP1 and -2); and soluble transferrin receptor (TFRC) were abundant in solid cellular granulomas (Fig. 1). In addition, the cellular regions of cavitory granulomas show a high abundance of ferritin (FTH/FL) and heme oxygenase (HMOX). Collectively, these are indicators of the cellular engagement in Fe uptake, Hb and heme-Fe recycling, and intracellular Fe storage, suggesting that

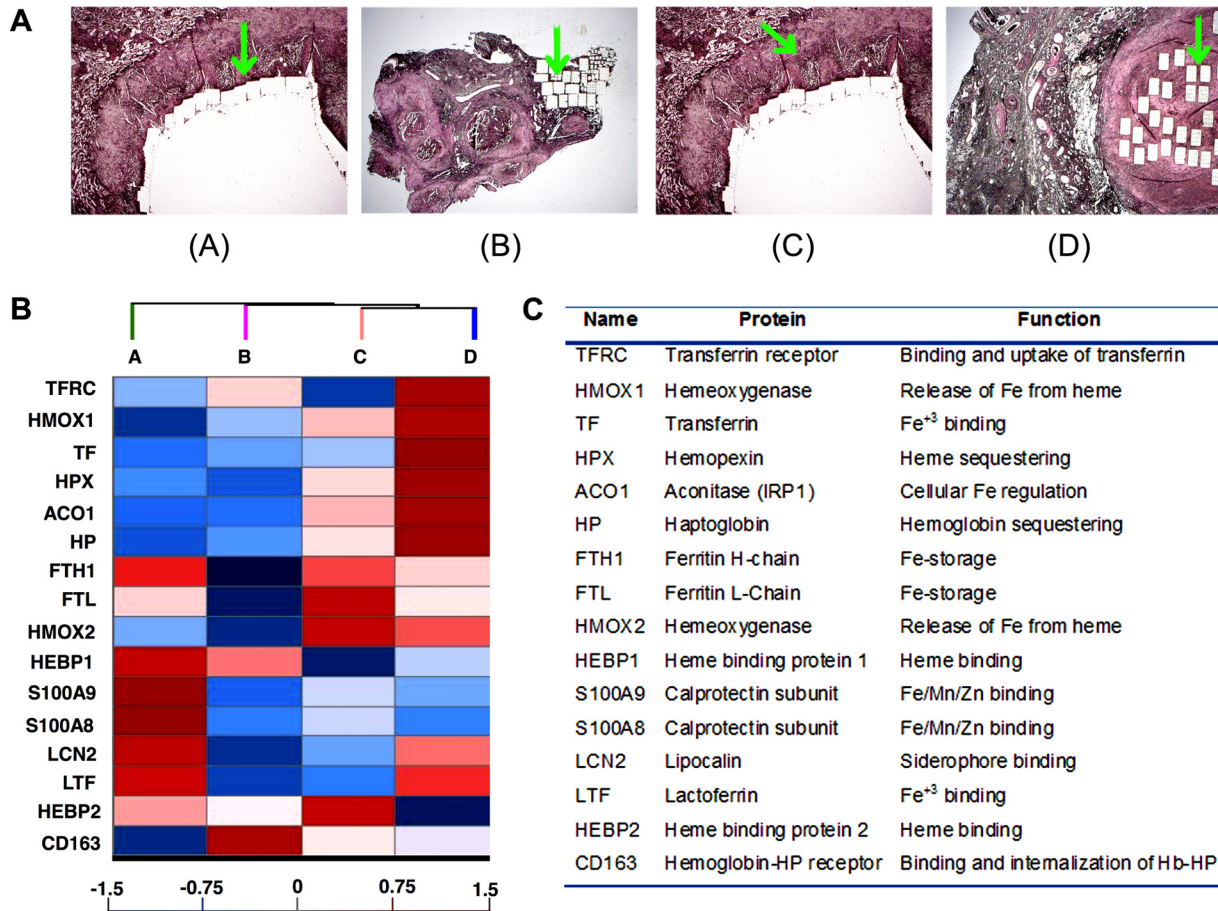


FIG 1 Proteomic analyses of host Fe-restricting proteins in human granulomas. (A) Histological sections of the types of granulomas sampled in the study pointing to the area dissected (green arrows): cavitory granuloma (necrotic region dissected) (A), solid granuloma (cellular region dissected) (B), cavitory granuloma (cellular region dissected) (C), and caseous granuloma (necrotic regions dissected) (D). (B) Heat map plot showing relative abundance of Fe-sequestering factors in the dissected areas of granulomas shown in panel A. (C) Proteins depicted in panel A and their function in iron metabolism.

M. tuberculosis may find a permissive Fe environment within these cells. In contrast, the necrotic center of a caseous granuloma showed accumulation of transferrin (TF), haptoglobin (HP), and hemopexin (HPX) (Fig. 1), which are potent extracellular sequestrers of Fe³⁺, Hb, and heme, respectively. Also abundant in necrotic areas were Fe-restricting antimicrobial proteins released by neutrophils upon degranulation, like Fe binding lactoferrin (LTF) (21) and lipocalin (LCN2), which sequesters siderophores and is involved in inhibition of mycobacterial growth *in vivo* (22, 23), and the metal chelator calprotectin (S100A9/S100A8) (24–26) (Fig. 1). Data analysis of an independent study of host gene expression in human granulomas compared to uninvolved tissue (27) showed a direct correlation between gene induction and abundance of Fe-sequestering proteins detected in the proteome of necrotic and cavitory granulomas, thus supporting an enhanced host Fe-restricting response in advanced TB granulomas (see Fig. S1 in the supplemental material). The concentration of basically all known Fe-restricting host proteins in the necrotic center of advanced granulomas suggests that bacteria might be subjected to intense Fe deprivation in this microenvironment. The high induction of Fe acquisition genes previously observed in *M. tuberculosis* isolated from infected human lungs is consistent with this interpretation (28).

***M. tuberculosis* persists under Fe starvation.** Considering the likely Fe deprivation of *M. tuberculosis* in necrotic granulomas, we examined how *M. tuberculosis* responds to conditions of strict Fe starvation. We established an *in vitro* model where *M. tuberculosis* was recovered from a frozen stock in standard 7H10 agar and transferred into Fe-

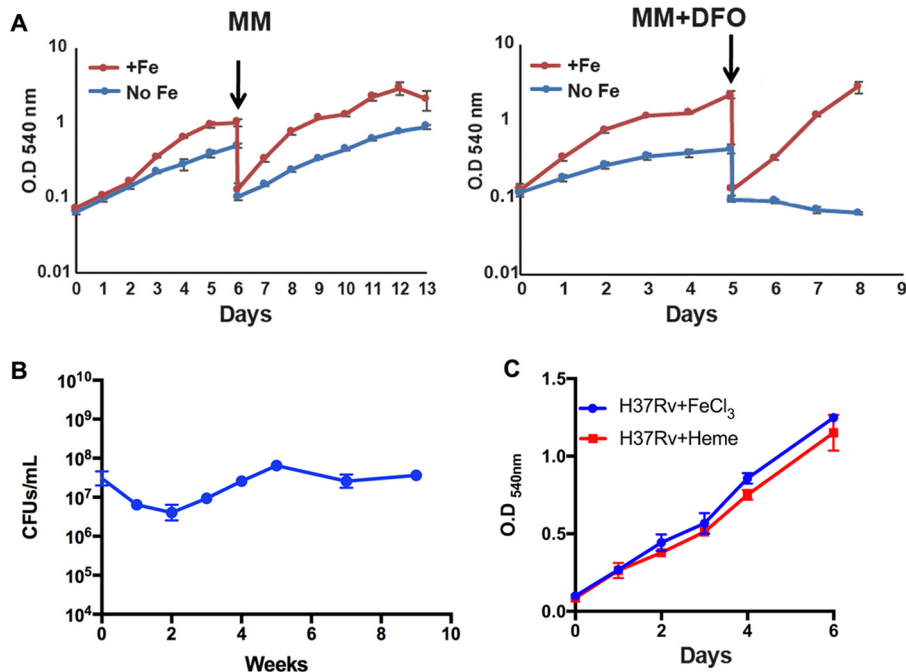


FIG 2 Iron starvation and persistence of *M. tuberculosis*. (A) *M. tuberculosis* was sequentially cultured in MM with FeCl₃ (+Fe) or in MM without Fe (No Fe) and MM+DFO. Growth was monitored based on the increase in optical density at 540 nm (OD₅₄₀). Black arrows indicate the time when the cultures were diluted. (B) Shown is the number of CFU per milliliter recovered after plating serial dilutions of MM+DFO cultures at indicated time points onto 7H10. (C) Fe-starving *M. tuberculosis* growth after culture supplementation with FeCl₃ or heme. Error bars represent means \pm standard deviations from three biological replicates.

depleted defined minimal medium (MM) and MM supplemented with deferoxamine (MM+DFO), a heterologous siderophore that chelates Fe³⁺ in the medium but is not taken up by *M. tuberculosis* (29). While the *M. tuberculosis* growth rate in MM was slightly reduced relative to cultures supplemented with FeCl₃, the cultures continued growing under these Fe-deficient conditions (Fig. 2A), possibly using traces of Fe in the medium and Fe stored within the cell (Fig. 2A). In contrast, the first pass of *M. tuberculosis* into MM+DFO resulted in a decreased growth rate, and the second pass into the same medium fully arrested *M. tuberculosis* growth (Fig. 2A). Although these Fe-starved mycobacteria ceased to grow, CFU enumeration by plating onto standard Fe-rich 7H10 medium showed that the cultures remained viable for over 9 weeks, the last time point examined (Fig. 2B). Furthermore, when the cells were provided with FeCl₃ or heme, they resumed normal replication (Fig. 2C). This remarkable ability to persist in the absence of exogenous Fe was not unique to *M. tuberculosis* H37Rv: other strains (Table 1), including *M. tuberculosis* Erdman and *M. tuberculosis* CDC1551, a recent clinical isolate (30), behaved similarly (Fig. S2).

TABLE 1 *M. tuberculosis* strains used in this study

<i>M. tuberculosis</i> strain	Description	Source or reference
H37Rv	<i>M. tuberculosis</i>	ATCC
Erdman	<i>M. tuberculosis</i>	ATCC
CDC1551	<i>M. tuberculosis</i>	30
H37Rv <i>dosR</i> mutant	$\Delta dosR::Kan$	34
H37Rv <i>mprA</i> mutant	<i>mprA::Kan</i>	I. Smith, unpublished data
H37Rv <i>sigE</i> mutant	<i>sigE::Kan</i>	72
H37Rv <i>sigB</i> mutant	<i>sigB::Kan</i>	85
H37Rv <i>bfrA</i> mutant	$\Delta bfrA::Hyg$	9
H37Rv <i>bfrB</i> mutant	$\Delta bfrB::Hyg$	9
H37Rv <i>clpB</i> mutant	$\Delta clpB::Hyg$	56

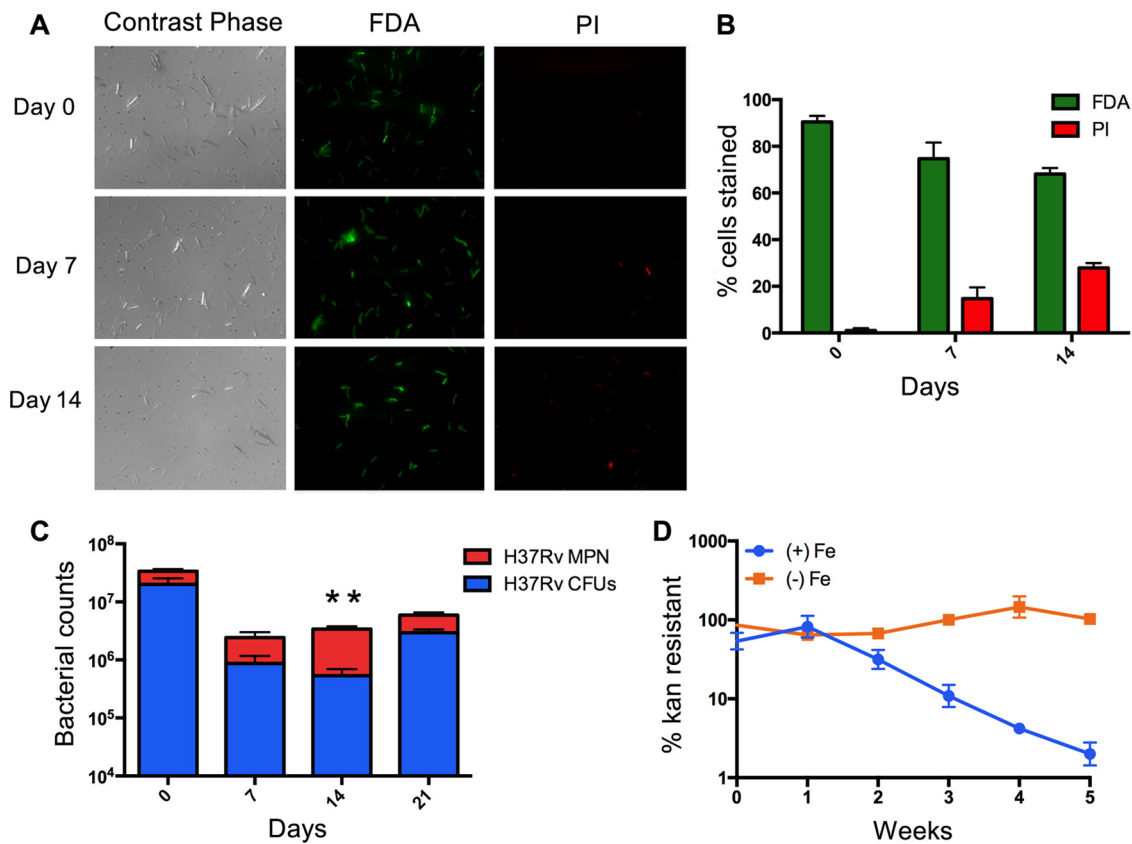


FIG 3 Phenotypic characterization of Fe-starving *M. tuberculosis*. (A) FDA and PI viability staining of growth-arrested MM+DFO *M. tuberculosis* cultures. (B) Quantification of the number of cells stained with FDA and PI. (C) Number of viable bacteria determined by MPN and CFU methods in MM+DFO cultures at indicated time points. (D) Percentage of Fe-starved growth-arrested *M. tuberculosis* that retained kanamycin resistance conferred by the replication clock plasmid PBP10. Error bars represent means ± standard deviations from three biological replicates. *, *P* value < 0.05; **, *P* value < 0.01.

During the first 2 weeks after growth cessation in MM+DFO, the number of CFU decreased 10- to 50-fold (Fig. 2B). However, at the same time the majority (~70 to 80%) of the cells stained positive for fluorescein diacetate (FDA) and negative for propidium iodide (PI) (Fig. 3A and B). FDA is a cell-permeant esterase substrate that measures both enzymatic activity, which is required to activate its fluorescence, and cell membrane integrity, which is required for intracellular retention of its fluorescent product. In contrast, the DNA-intercalating agent PI cannot pass through an integral cell membrane (Fig. S3). Thus, the results indicated that most Fe-starving cells were metabolically active and had an intact cell envelope. To address this discrepancy in viability measurements produced by different methods, we employed the most probable number (MPN) dilution culture method (31) and enumerated bacteria that grow in 7H9 broth. In agreement with the viability staining, the MPN method showed a larger number of viable cells than the CFU method (Fig. 3C), indicating that the MM+DFO culture contained a population of bacteria that remained viable but failed to produce colonies on 7H10 agar. Such differentially culturable bacterial cells (DCCs) have been detected during stress as well as in sputum produced by TB patients (32). However, to the best of our knowledge, this is the first time that *M. tuberculosis* DCCs have been associated with Fe deficiency.

After the 2nd week of culture in MM+DFO, the size of the DCC population decreased while the CFU numbers increased and stabilized (Fig. 2B and 3C). We termed this population “iron-starved growth-arrested *M. tuberculosis*” (ISGAM). We found that ISGAM showed enhanced tolerance to several antibiotics, including isoniazid (INH), a first-line TB drug (Table 2). However, they remained as equally sensitive to rifampin as Fe-sufficient bacteria, indicating that DNA transcription is required for acclimation to Fe starvation.

TABLE 2 Differential antibiotic sensitivity in Fe-starving growth-arrested *M. tuberculosis* and Fe-sufficient bacteria

Antibiotic	MBC ₉₀ (μg/ml) on culture ^a :	
	MM+DFO	MM plus Fe
Ciprofloxacin	>16	1
Cycloserine	>200	12.50
Ethionamide	>40	1.20
Isoniazid	10	0.30
Kanamycin	>25	6.20
Rifampin	0.06	0.06

^aThe MBC₉₀ was determined for biological triplicates of MM+DFO and MM-plus-Fe *M. tuberculosis* cultures.

To assess whether ISGAM was equivalent to a nonreplicative state, we used a “replication clock”—an unstable plasmid that is lost at a constant rate per cell division (33). We found that ISGAM retained the plasmid (as determined by resistance to kanamycin) for up to 5 weeks, indicating very little or no replication (Fig. 3D). Collectively, these results demonstrate that the *M. tuberculosis* response to Fe deprivation—a condition that it might encounter in necrotic granulomas—is dynamic and includes phases of cell death, differential culturability, and nonreplicative persistence.

Transcriptional and metabolic responses of Fe-starving *M. tuberculosis*. ISGAM’s transcriptional and metabolic profiles were analyzed to investigate the mechanisms of persistence under Fe starvation. Differential gene expression detected in microarrays (Fig. 4) was generally confirmed by transcriptome sequencing (RNA-seq) (Fig. S4 and Data Set S1D). Although growth-arrested cells repressed macromolecular synthesis and growth genes, a few hundred gene transcripts encompassing several functional categories (Table S1) were more abundant in ISGAM than in Fe-replete cells (≥ 2.0 -fold

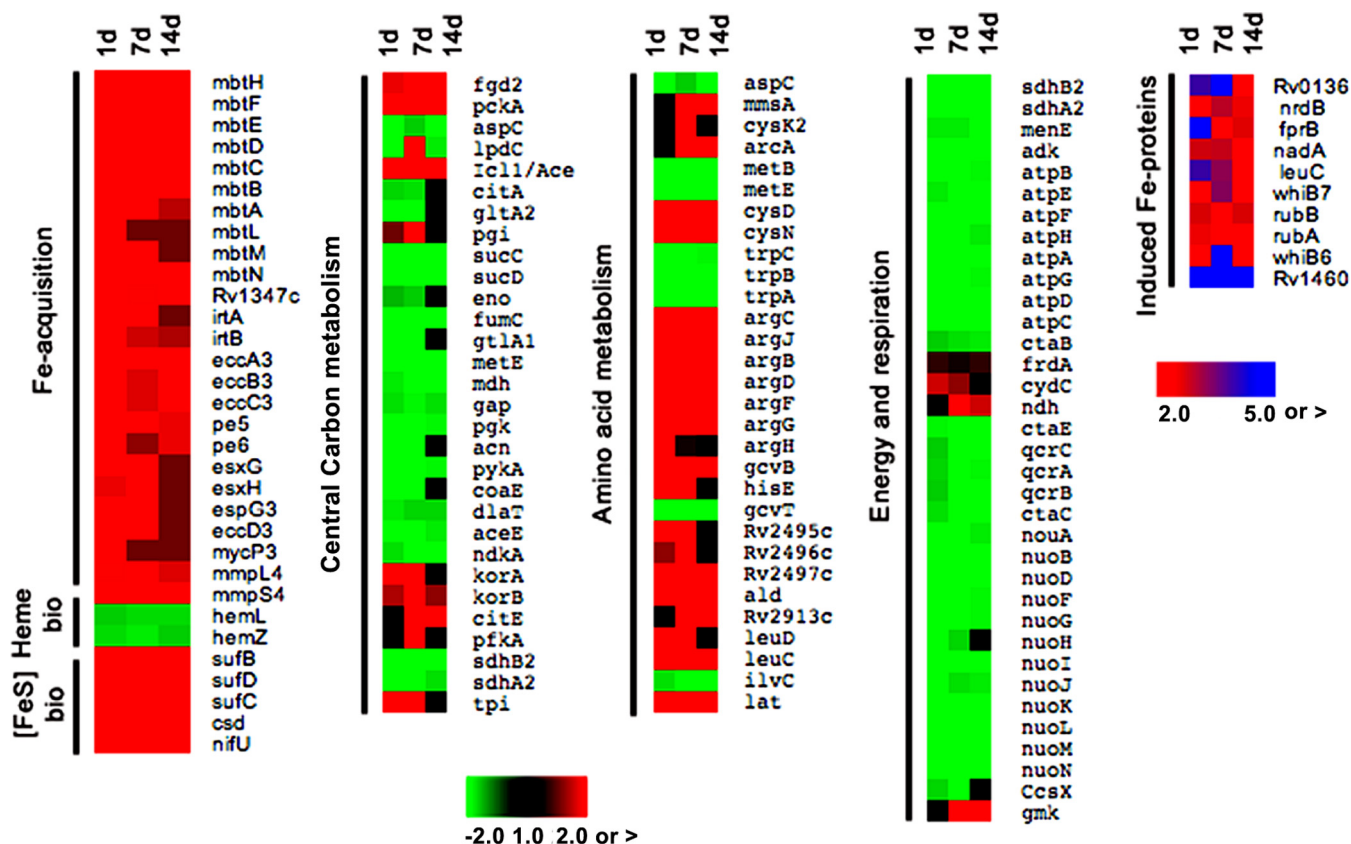


FIG 4 Time course transcriptional profile of Fe-starved *M. tuberculosis*. Triplicate *M. tuberculosis* cultures from three independent experiments were harvested at days 1, 7, and 14, and RNA was extracted. *P* values for heat maps can be found in the GEO database (accession number GSE84554).

TABLE 3 Metabolite abundance of Fe-starving and Fe-sufficient *M. tuberculosis*

Process and metabolite	Fold change, –Fe/+Fe ^a
Glycolysis	
Glucose-6-phosphate	0.02
Pyruvate	5.50
TCA cycle	
Citrate	4.10
α -Ketoglutarate	1.60
Succinate	0.60
Fumarate	2.90
Malate	0.02
Amino acid metabolism	
Threonine	0.30
Lysine	2.10
Amino adipate	9.10
N-Acetyl-lysine	2.40
Methionine	0.04
S-Adenosylmethionine (SAM)	0.20
Glutamate	0.13
N-Acetyl-ornithine	21
Ornithine	1.80
Citrulline	0.09
Arginine	2.10
Valine	1.20
Histidine	0.50

^aValues correspond to the average metabolite ratio between 1-day MM+DFO (–Fe) and 1-day Fe-replete cultures (+Fe). The *P* value of the fold change for all metabolites in the table is <0.05.

change, with a false discovery rate [FDR] of ≤ 0.01). However, over 20% of induced genes encoded proteins of unknown function, highlighting a yet-unknown component of the Fe starvation response.

A comparison of the ISGAM transcriptional profile with those reported for nonreplicating *M. tuberculosis* under oxygen depletion (34) and nutrient-starved *M. tuberculosis* (35) and with the common expression profile of those conditions and stationary-phase *M. tuberculosis* (36) identified 124 genes commonly induced in Fe starvation and at least one other growth-limiting condition (Data Set S1A and B), while ~240 genes were induced only in Fe starvation (Data Set S1C). Thus, with the caveat that parallel experimental comparisons are the best way to define a condition-specific gene signature, the *M. tuberculosis* response to Fe starvation appears to have a unique gene expression component that is also reflected in the metabolic activity of ISGAM as described below.

(i) Economics of Fe in ISGAM. Fe-starving bacteria maintained a high abundance of Fe-acquisition gene transcripts for at least 14 days, the last time point examined, indicating that they continued trying to obtain Fe (Fig. 4). They also upregulated essential Fe-S cluster [Fe-S] assembly genes (*suf*) (37) while reducing synthesis of heme and most, but not all, Fe proteins (Fig. 4). These changes are consistent with an active Fe-sparing response—a coping strategy in which cells prioritize the use of scarce Fe by repressing the synthesis of dispensable Fe proteins (38). Thus, the *M. tuberculosis* Fe-sparing response seems to prioritize [Fe-S] biogenesis over heme synthesis and synthesis of Fe proteins involved in electron transfer (Cyp138, FprB, RubA, and RubB), NAD synthesis (NadA), and the [Fe-S]-dependent regulators WhiB6 and WhiB7 (39–42) (Fig. 4).

(ii) Metabolic challenges associated with Fe restriction. Both the transcriptional and metabolomic profiles indicated that amino acid and central carbon metabolism were significantly affected by Fe starvation (Fig. 4; Table 3). Genes encoding enzymes of the tricarboxylic acid (TCA) cycle and oxidative phosphorylation were mostly repressed, which is not unexpected given the number of [Fe-S]/heme proteins involved in these pathways (Fig. 4). Concomitantly, expression of *atp* genes (encoding F_1F_0 ATP

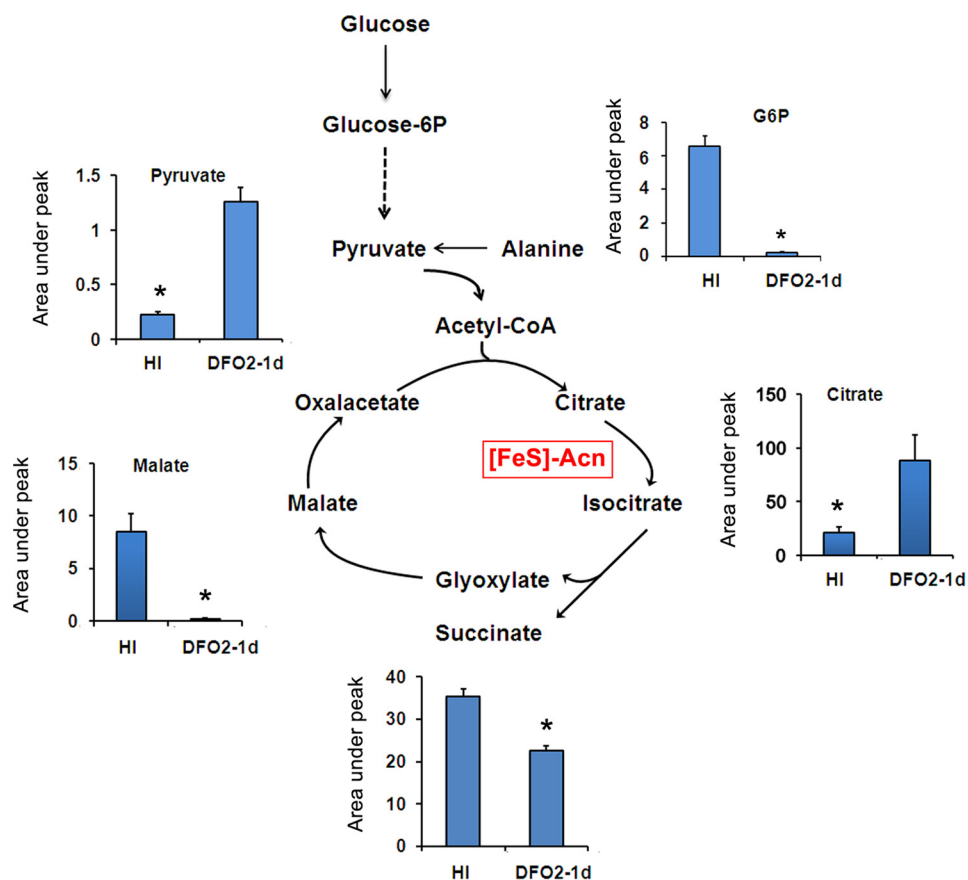


FIG 5 *M. tuberculosis* metabolic reprogramming during Fe starvation. Diagram showing abundance of intermediate metabolites of glycolysis, TCA, and glyoxylate cycle in Fe-replete cultures (HI) and MM+DFO cultures at 1 day into Fe starvation (DFO2-1d). The values represent the areas under the peak normalized to cell number in each sample. Error bars represent the SDs from biologically independent triplicates. *, *P* value < 0.05. CoA, coenzyme A.

synthase) was decreased (Fig. 4), indicating reduced respiration-associated ATP synthesis. Furthermore, we found that ISGAM repressed expression of aconitase, the [Fe-S] enzyme that catalyzes the isomerization of citrate to isocitrate, the substrate for the TCA cycle and the glyoxylate shunt (GS) (Fig. 4 and 5). Consistent with a metabolic roadblock at this step, ISGAM accumulated high levels of citrate (Fig. 5). We also observed a decrease in cellular levels of glucose-6-phosphate and repression of glycolytic genes (Fig. 4 and 5), indicating a downregulation of glycolysis. Nevertheless, pyruvate levels increased in ISGAM (Fig. 5), suggesting a different origin for pyruvate. One possible source is alanine, since alanine dehydrogenase (Ald), the enzyme that produces pyruvate from Ala with concomitant reduction of NAD to NADH (43), was highly upregulated in ISGAM (Fig. 4).

Consistent with downregulation of the methionine biosynthetic genes *metC*, *metB*, *metE*, and *metA* (Fig. 4), the levels of methionine and the methionine derivative *S*-adenosylmethionine (SAM) decreased (Table 3), suggesting impaired SAM-dependent catalysis in Fe-starving *M. tuberculosis*.

While the levels of most amino acids decreased in ISGAM, lysine, which serves as a siderophore building block (44), and arginine increased (Table 3). The increase in arginine paralleled the upregulation of the entire *arg* gene cluster (Fig. 4), a decrease in the precursor amino acid glutamate, and an increase in other metabolites of this pathway, including *N*-acetyl-ornithine, ornithine, and fumarate (Table 3) (45).

Genes encoding enzymes involved in mycolic acid and cell wall dimycoserate ester (DIMs) biosynthesis were downregulated, while genes necessary for cholesterol catabolism (46) and persistence in the host (47) were upregulated in ISGAM (Fig. S5A).

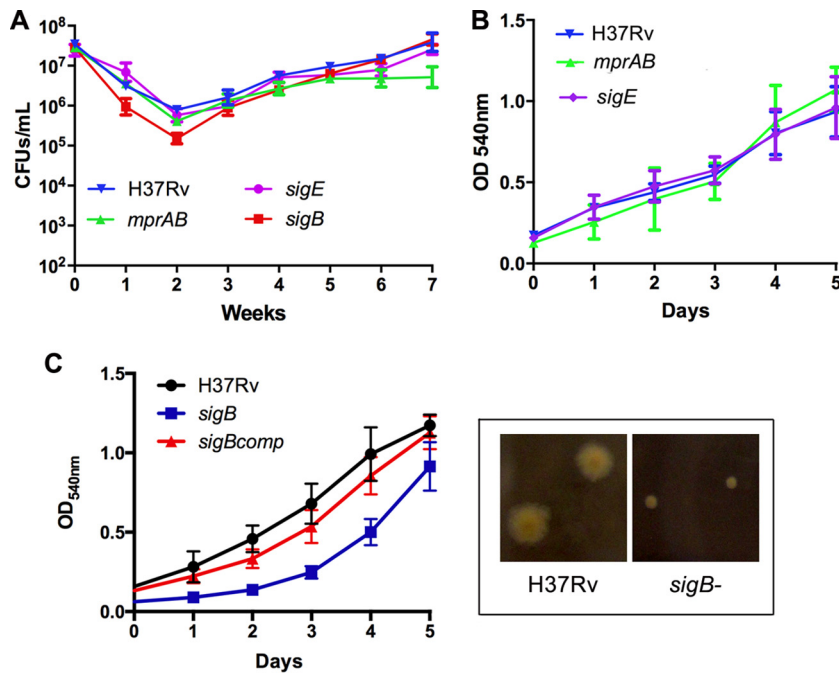


FIG 6 Persistence of *mprA*, *sigE*, and *sigB* *M. tuberculosis* mutants under Fe starvation. (A) Shown is the number of CFU per milliliter recovered after plating serial dilutions of MM+DFO cultures of *M. tuberculosis* mutant strains onto 7H10 agar. (B) Growth of Fe-starving *mprA* and *sigE* mutant *M. tuberculosis* strains supplied with Fe. (C) Growth of Fe-starving *sigB* *M. tuberculosis* mutant upon Fe addition. The micrograph shows same-age colonies produced by *M. tuberculosis* wild type and *sigB* mutant on 7H10 agar. Data are expressed as the means \pm standard deviations from three biological replicates.

ISGAM cells also stained positive with Nile red, suggesting accumulation of neutral lipids during Fe starvation (Fig. S5B).

Genetic determinants of ISGAM viability and recovery. We next examined survival and recovery of *M. tuberculosis* gene knockout mutants to identify genes and pathways important for survival or recovery from Fe starvation.

(i) Regulators of gene expression. The transcriptomic analyses showed the cell surface stress response network composed of the two-component system MprAB and the sigma factors SigE and SigB (48) being induced during Fe starvation, suggesting surface stress secondary to Fe deficiency in *M. tuberculosis*. Inactivation of *mprA* or *sigE* did not affect survival or recovery from Fe starvation, but the Fe-starved *sigB* mutant produced significantly smaller colonies on 7H10 and its recovery in Fe-supplemented MM was delayed (Fig. 6), indicating *mprAB*- and *sigE*-independent *sigB* expression during Fe deficiency and a role for the *sigB* regulon during recovery from Fe starvation.

A distinctive feature in the transcriptional response to Fe starvation was low or no induction of the majority of genes in the dormancy regulon, approximately 50 genes induced under oxygen limitation or exposure to nitric oxide and activated by the dormancy survival regulator (DosR) (34, 49, 50). Accordingly, a *dosR* mutant (34) survived and recovered from Fe starvation normally (Fig. S6), confirming the dispensability of the DosR regulon for persistence in the absence of Fe.

(ii) Fe storage proteins. It has been recognized that in early stages of infection within naive macrophages, *M. tuberculosis* manipulates the phagosome to gain access to incoming Fe and that it obtains sufficient Fe via siderophores for replication and storage (9, 51–54). In our model, bacteria are recovered from frozen stocks in Fe-containing 7H10 agar, and therefore, they too can store Fe. *M. tuberculosis* encodes two iron storage proteins, a heme-containing bacterioferritin (BfrA) and a ferritin-like protein (BfrB). BfrB seems to be the housekeeping Fe storage protein in *M. tuberculosis*, while BfrA is needed under some stress conditions (9). BfrB is also needed for *M. tuberculosis* survival during the chronic phase of infection in mice, and a *bfrB* mutant

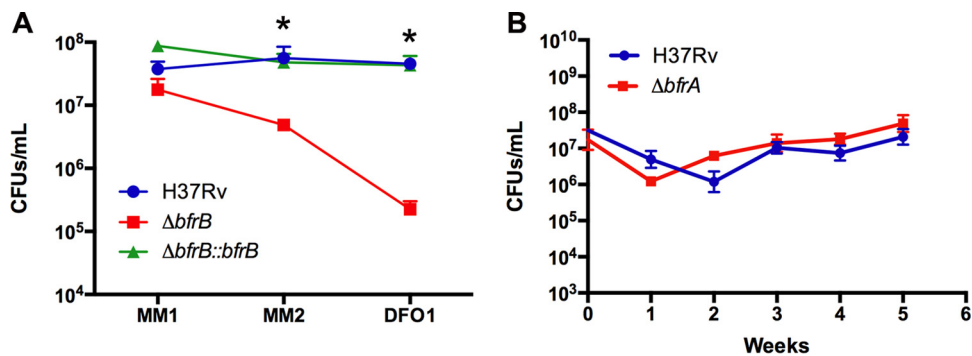


FIG 7 Survival of Fe storage mutants under Fe starvation. (A) CFU of wild-type and $\Delta bfrB$ and $\Delta bfrB$ -complemented strains recovered in the initial phases of Fe depletion in MM and the first passage in MM+DFO. Wild-type and *bfrB*-complemented mutant strains grew during each passage; therefore, the CFU number in the graph was obtained by plating dilutions of cultures adjusted to an OD₅₄₀ of 0.1. (B) CFU of wild-type and $\Delta bfrA$ mutant in MM+DFO. Error bars represent means \pm standard deviations from three biological replicates. *, *P* value < 0.05.

shows hypersensitivity to oxidative stress and antibiotics (9). We investigated the requirement of stored Fe for acclimation to Fe starvation using isogenic *bfrA* and *bfrB* mutant strains of *M. tuberculosis*. A ferritin mutant ($\Delta bfrB$) showed an ~ 3 -log loss of viability during the initial phases of Fe depletion in MM, while a bacterioferritin mutant ($\Delta bfrA$) was not affected (Fig. 7), indicating that *M. tuberculosis* depends on Fe stored in ferritin to survive. This result suggests that the size of the Fe storage pool may be a determinant of whether the bacteria can successfully adjust to Fe starvation.

(iii) Regulators of proteostasis. Our transcriptomics and metabolomic analyses suggested that efficient recycling and reuse of Fe from nonessential proteins and essential protein recycling might be critical for enduring Fe starvation. To test this prediction, we interrogated the transcriptomics data for upregulated genes encoding proteins that might facilitate these processes. We found that *clpB*, which encodes a chaperone that helps disaggregate misfolded proteins and sequesters those that are irreversibly damaged (55, 56), was highly induced in ISGAM at all time points tested (2.1-, 4.5-, and 5.6-fold at 1, 7, and 14 days, respectively). Therefore, we examined the effect of *clpB* inactivation (56) on *M. tuberculosis* persistence. CFU recovered from the *clpB* mutant decreased drastically during Fe starvation (Fig. 8), suggesting an important

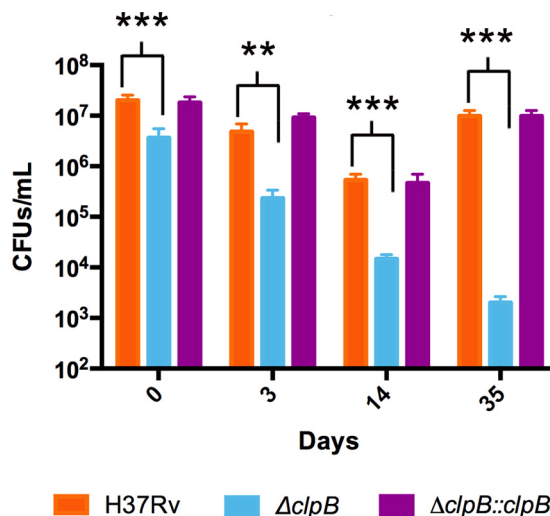


FIG 8 Survival of a *clpB* mutant subjected to Fe starvation. Shown are the CFU of wild-type, $\Delta clpB$ mutant, and $\Delta clpB$ -complemented *M. tuberculosis* MM+DFO cultures at indicated times. Error bars represent means \pm standard deviations from three biological replicates. *, *P* value < 0.05; **, *P* value < 0.01; ***, *P* value < 0.001.

role for ClpB-mediated proteostasis in enduring Fe deprivation.

DISCUSSION

This study showed that the necrotic center of human granulomas has a high concentration of Fe-sequestering proteins and Fe-restricting factors, likely establishing an Fe-deprived environment for the infecting *M. tuberculosis*. We also showed that *M. tuberculosis* has a remarkable ability to persist for a long time under conditions of Fe deprivation with little or no replication, refractive to antibiotics and capable of resuming normal growth when Fe is restored. Our findings raise the possibility that an effective nutritional immunity might also promote establishment of chronic TB. This expands the current view of the host responses to infection that might trigger quiescence of *M. tuberculosis* and provides new opportunities to identify metabolic vulnerabilities of persistent bacteria that can be targeted for new therapeutics.

Our results revealed that Fe starvation triggers the appearance of bacilli that, although viable, were unable to form colonies on agar plates. *M. tuberculosis* isolates exhibiting a similar differentially culturable cell (DCC) phenotype have been detected in sputum samples from TB patients prechemotherapy (57), indicating that they occur *in vivo* and are therefore extremely important in culture-based diagnostics and evaluation of treatment efficacy. Nonetheless, they are poorly characterized due in part to the difficulties involved in detecting them. Since DCCs emerge in a highly reproducible manner in Fe-starving cultures, the *in vitro* model established here could be valuable to further understand the physiology of this bacterial population. In addition, our results suggest a high probability that some transmitted bacilli are Fe deficient. This might influence initial host pathogen interactions as infecting bacilli must regain access to Fe to establish a new productive infection. Indeed, we found that Fe deficiency induces expression of genes needed for subversion of macrophage antimicrobial defense, such as the type VII secretion system Esx-3, and the protein kinase PknG and other virulence-associated factors, including sulfolipid biosynthesis, cholesterol utilization genes, isocitrate lyase, phosphoenolpyruvate carboxykinase, and WhiB6 (47, 58–61). Collectively, these observations support the idea that *M. tuberculosis* coordinates the response to Fe limitation with expression of factors that enable survival in the host.

Fe-starving growth-arrested *M. tuberculosis* shows reduced sensitivity to several antibiotics, including the first-line TB drug isoniazid (INH), also used in preventive therapy against LTBI reactivation. One explanation for this observation is that non-growing cells contain a reduced abundance of the drug target. However, Fe deficiency may also specifically contribute to antibiotic tolerance. For instance, INH is a prodrug activated by catalase (KatG), a heme enzyme (62, 63). Since *katG* is downregulated ~2.0-fold under Fe starvation, reduced drug activation may contribute to ISGAM's INH tolerance. In addition, inhibition of the electron transport chain due to Fe deficiency likely mediates enhanced tolerance to aminoglycoside antibiotics, which require an active electron transport chain to enter the cell. Furthermore, the genes encoding recognized intrinsic antibiotic resistance enhancers, such as WhiB6 (40), WhiB7 (42), and the fluoroquinolone efflux pump encoded by Rv2688c (64), are also induced in response to Fe deficiency, supporting an active role of the Fe-deficiency response in antibiotic tolerance. Given these results, we believe that Fe-limited *M. tuberculosis* constitutes a valuable screening platform for new antitubercular antibiotics.

In trying to understand the essential metabolic reprogramming of Fe-starving *M. tuberculosis*, we sought out parallels with *Lactobacillus* sp. and *Borrelia burgdorferi*, which are exceptional in that they exist and proliferate without Fe (65, 66). These bacteria have no [Fe-S] assembly genes, and the *B. burgdorferi* genome does not encode enzymes of the TCA cycle or oxidative phosphorylation—pathways that depend largely on [Fe-S]/heme proteins. Both of these bacteria rely on substrate phosphorylation for production of ATP (66) and depend on pyruvate conversion to lactate via lactate dehydrogenase to regenerate NAD⁺ required for continued glycolysis. Metabolic detection of lactate in ISGAM suggests that *M. tuberculosis* performs homo-lactic fermentation during Fe starvation; however, further analyses are needed to

decipher the metabolic sources of energy in ISGAM. *Lactobacillus* and *Borrelia* also use Mn^{2+} instead of Fe^{2+} as a cofactor of several essential enzymes. Mycobacteria also show indications of employing this strategy. For instance, the superoxide dismutase SodC, which is essential to resist exogenous oxidative stress, is a Cu,Zn enzyme (67). Thus, it is possible that over its long coexistence with humans experiencing Fe limitation, *M. tuberculosis* has evolved cambialistic enzymes and/or learned to use alternative available cofactors.

Interestingly, we found that ISGAM did not accumulate succinate, which is accumulated in *M. tuberculosis* under hypoxic conditions (68). Secretion of succinate, derived from isocitrate cleavage, is thought to help *M. tuberculosis* maintain a proton motive force under respiratory stress caused by oxygen depletion (68, 69). Instead, we found that citrate and fumarate increase in Fe-starving *M. tuberculosis* (Fig. 5), suggesting that ISGAM and oxygen-depleted nonreplicative *M. tuberculosis* use distinct mechanisms to maintain an energized membrane. The specific nature of these mechanisms is under investigation.

Our findings regarding the marked increase in arginine biosynthesis during Fe starvation are very intriguing, particularly in the context of recent discoveries of the role of arginine as a metabolic regulator of survival of activated T cells (70) and as a metabolic cue in intraspecies communication in bacteria. L-Ornithine, an arginine synthesis intermediate exported by *Enterococcus faecalis*, a pathogen involved in polymicrobial pathogenesis, stimulates *Escherichia coli* to synthesize enterobactin, a siderophore needed for biofilm formation under iron-limiting conditions (71).

This study identified two cellular processes important for persistence under Fe starvation: Fe storage in ferritin (BfrB) and ClpB-mediated proteostasis. The $\Delta bfrB$ survival defect suggests that shutting down growth before Fe reserves in ferritin are exhausted is necessary to maintain viability during Fe deprivation. Thus, it is possible that a reduced Fe-ferritin pool may signal poor nutritional conditions leading to activation of cell growth control mechanisms in *M. tuberculosis*. BfrB and ClpB were previously shown to be important also for *M. tuberculosis* replication *in vivo* (9, 56). Together with our study, these results indicate that these proteins constitute good targets for developing antimicrobials effective against both replicating and persistent *M. tuberculosis*.

The World Health Organization estimates indicate that 1.6 billion people, over 25% of the world's population, suffer anemia, mainly due to Fe deficiency (86). These numbers, the adverse effects of Fe repletion on the course of TB, and the results of this study underscore the need for careful monitoring of Fe supplementation programs in areas where TB is endemic. Collectively, they also lend support to the intriguing theory that Fe deficiency may be part of an evolutionary compromise permitting optimum coexistence of host and pathogen (15).

MATERIALS AND METHODS

Bacterial strains, media, and growth conditions. Bacterial strains and plasmids used in this study are listed in Table 1. *M. tuberculosis* strains were recovered from frozen stocks on Middlebrook 7H10 agar (Difco) supplemented with 0.5% (vol/vol) glycerol, 0.05% Tween 80, and 10% (vol/vol) albumin-dextrose-NaCl complex (ADN). Fe-depleted minimal medium (MM) was used for iron starvation experiments. MM contains 0.5% (wt/vol) asparagine, 0.5% (wt/vol) KH_2PO_4 , 2% glycerol, 0.05% Tween 80, and 10% ADN, and its pH was adjusted to 6.8 with NaOH. To remove metal ions, MM was treated with 5% Chelex-100 (Bio-Rad) for 24 h at 4°C with gentle agitation. The Chelex-100 resin was removed by filtration through a 0.22- μm filter (Millipore), and the medium was supplemented with 0.5 mg of sterile $ZnCl_2$ liter⁻¹, 0.1 mg of $MnSO_4$ liter⁻¹, and 40 mg of $MgSO_4$ liter⁻¹. The amount of residual Fe in this medium, determined by atomic absorption spectroscopy, is $\sim 1 \mu M$. The *M. tuberculosis mprA* mutant used in this study was a kind gift from Issar Smith (PHRI, Newark, NJ), and it was obtained by insertion of a Kan^r cassette (*aph*) in the *mprA* gene via homologous recombination using the suicide plasmid PSM270 (72). Disruption of the gene was confirmed by PCR analysis (see Fig. S7 in the supplemental material).

Proteomic analysis of human lung tissues. The proteomic analyses of human lung tissues were described previously (19). Briefly, tubercular lung tissues were removed from participants who had undergone therapeutic lung resection surgery at the National Masan Hospital (NMH; South Korea). The patients had been infected with multidrug-resistant (MDR) TB and were treatment refractory to second-line drug therapy. The tissue collection has been described previously (73) and was approved by the NMH institutional review board, and an exemption for studying the archived tissues was granted by NIH,

with written consent of the subjects; samples collected between 2002 and 2008 were deidentified when provided for dissection. The lung tissues were from a set of six participants and largely displayed three types of pathological structures, namely, solid cellular granulomas, caseous granulomas, and cavitory granulomas. To obtain histologically distinct compartments, necrotic (caseum) and cellular (cell) regions were dissected from each granuloma type with the Laser Pressure Catapulting (LPC) Palm instrument (Zeiss, Göttingen, Germany). Dissected tissues were lysed and subjected to in-gel digestion (Lys-C protease and trypsin) and peptide extraction. Liquid chromatography-tandem mass spectrometry (LC-MS-MS) analysis of resulting peptides was performed as single-shot runs, using a Q-Exactive mass spectrometer (Thermo Fisher Scientific) coupled online with a nanoflow ultra-high-pressure liquid chromatography (UHPLC) instrument (Easy nLC; Thermo Fisher Scientific). Protein quantification was performed as described previously (19, 74). Mass spectra were analyzed using the MaxQuant computational platform version 1.3.0.5 and Andromeda against the UniProt FASTA human database, and proteome quantification was performed in MaxQuant using the XIC-based inbuilt label-free quantification (LFQ) algorithm as previously described (19).

The abundance of proteins was based on the relative quantification of a protein in a given dissected histological region compared to all other samples subjected to proteomics. The normalization utilized in the label-free quantification exploits the fact that there are dominant populations of proteomes that do not change between experimental conditions or samples, so that their average behavior can be used as a relative standard. Thus, the abundance is determined relative to a standard that is derived from common peptides/proteins that change minimally between experimental conditions.

We analyzed proteins associated with Fe metabolism from these data that are publicly available and have been deposited into the PRIDE partner repository with the data set identifier PXD003646, which can be accessed from the Proteome Xchange Consortium (<http://proteomecentral.proteomexchange.org>). The heat map plot was constructed from Z score- and \log_2 -transformed LFQ protein intensities.

Analyses of host Fe metabolism gene expression in human granulomas. Expression of Fe homeostasis host genes in the cellular region adjacent to necrotic-cavitory granulomas was analyzed in comparison to uninvolved tissue isolated from the lungs of human TB patients from publicly available data (GEO accession number [GSE20050](https://www.ncbi.nlm.nih.gov/geo/query/acc.cgi?acc=GSE20050)). Acquisition of lung tissue, processing of the samples, and DNA microarray analysis were reported previously (27).

Iron starvation procedure. To minimize Fe contamination from glass, plastic containers were exclusively used. An exponentially growing *M. tuberculosis* strain revived from a frozen stock on a 7H10 agar plate was inoculated into 5 ml of MM at an initial optical density at 540 nm (OD_{540}) of 0.1 in 15-ml polypropylene tubes and incubated at 37°C, with constant agitation, in a cell culture rotator to early stationary phase (OD_{540} of ~1). MM cultures were diluted to an OD_{540} of 0.1 in the same medium and allowed to grow to early stationary phase to deplete stored Fe and then diluted to an OD_{540} of 0.1 in MM containing 50 $\mu\text{g ml}^{-1}$ of freshly prepared deferoxamine mesylate (Sigma). This culture replicated slowly and reached a maximum OD_{540} of 0.35 to 0.40. At this point, the culture was divided in two and diluted to an OD_{540} of 0.1 in the same medium or in MM containing 50 $\mu\text{M FeCl}_3$ (Fe-replete culture). The MM+DFO culture ceased to grow, and therefore, it was maintained for phenotypic studies while the Fe-replete culture was collected 24 h afterward and used as a reference for microarray and metabolite analyses. The growth-arrested MM+DFO cultures are referred to here as Fe-starved growth-arrested *M. tuberculosis* (ISGAM).

Determination of cell viability. At various time points, 10-fold serial dilutions of ISGAM cultures were made and plated onto 7H10 agar to enumerate CFU. Live/dead staining with fluorescein diacetate (FDA) and propidium iodide was used to distinguish living cells from the dead-cell population.

For FDA and PI staining, 1 ml of culture was centrifuged, and the pellet was resuspended in 1 ml of phosphate-buffered saline (PBS)–0.02% Tween 80 and stained with FDA (final concentration, 10 $\mu\text{g ml}^{-1}$) and PI (final concentration, 4 $\mu\text{g ml}^{-1}$) for 20 min, at room temperature, in the dark. Samples were centrifuged and washed once with PBS-0.02% Tween 80, fixed with 8% paraformaldehyde, and concentrated to 0.1 ml by centrifugation. Five microliters of the sample was added to a 1% agarose pad, placed on a poly-D-lysine-coated Fluorodish (Time Precision Instruments), and visualized on an Axiovert 200 M inverted fluorescence microscope (Zeiss), equipped with a CoolSNAP HQ camera (Photometrics, Pleasanton, CA). Images were acquired with OPENLAB acquisition software (Improvision, Sheffield, United Kingdom).

Recovery from Fe starvation in liquid medium. At the desired time point, DFO was removed from Fe-starving cultures by centrifugation. The bacterial pellet was resuspended in MM supplemented with 80 $\mu\text{M FeCl}_3$ or MM-DFO as a control and incubated at 37°C with agitation. Growth was monitored by measuring the increase in optical density.

For most probable number (MPN) determinations, 10-fold serial dilutions from three independent cultures were made up to a 10^{-7} dilution and 100 μl of each dilution was added to 1.9 ml 7H9 in a 5-ml polystyrene round-bottom tube. For each dilution, there were five replicate tubes. The tubes were incubated at 37°C for 2 months. Tubes with visible turbidity were counted as positive, and MPN was calculated using standard statistical methods (31).

Antibiotic sensitivity assays. Sequential dilutions of ISGAM and Fe-sufficient *M. tuberculosis* cultures were treated for 3 days with increasing concentrations of several antibiotics. After treatment, the cultures were serially diluted in 7H9 and 5 μl of each dilution was spotted on 7H10 plates. Cells not treated with antibiotics were also spotted in the same plates as a control. We report MBC_{90} , which is the concentration of drug that resulted in 90% reduction in the CFU of the treated culture compared to the untreated control.

RNA extraction and bacterial transcriptomic analyses. ISGAM cultures were collected at 1, 7, and 14 days, Fe-replete cell cultures were collected at day 1 and centrifuged at 4,500 rpm for 5 min, and the cell pellets were resuspended in 1 ml TRI reagent and immediately transferred to a tube containing 0.5 ml of 200- μ m zirconia beads (Sigma-Aldrich) and disrupted by two 1-min pulses in a BeadBeater. RNA was purified as previously described (75) using RNeasy columns according to the manufacturer's instructions (Qiagen). The quality and quantity of purified RNA were estimated using a NanoDrop spectrophotometer (NanoDrop, Wilmington, DE). Total RNA was isolated from triplicate cultures and three independent experiments.

Microarray analysis was performed as previously described (76). The *M. tuberculosis* DNA microarray consisted of 4,295 70-mer oligonucleotides representing the 3,924 predicted open reading frames (ORFs) of the H37Rv strain (<http://www.sanger.ac.uk>). The arrays were prepared by spotting oligonucleotides (tuberculosis genome set version 1.0; Operon Biotechnologies) onto poly-L-lysine-coated glass microscope slides, using a GeneMachines Omnigrid 100 Arrayer (Genomic Solutions) and SMP3 pins (Telechem) as described above. Briefly, cDNA was synthesized using random primers and labeled with Cy3- or Cy5-dUTP (PerkinElmer) as described before (48) and hybridized to the arrays overnight. After washing, the arrays were scanned with a GenePix 4000B scanner (Molecular Devices). The images were processed using GenePix 5.1. Data were filtered by removing all spots that were not above the background noise. Spots were considered to be not sufficiently above background noise for further analysis if the sum of the median intensities of the two channels was less than twice the highest mean background of the chip. The chips were normalized by the print-tip LOWESS method (77). The ratio of the mean median intensity of Cy5 to the mean median intensity of Cy3 was determined for each spot, and the fold change values were calculated.

RNA sequencing. RNA from biological triplicates of ISGAM cultures at 1 and 7 days and from Fe-replete *M. tuberculosis* cultures was isolated using the Directzol RNA extraction kit (Zymo Research) according to the manufacturer's instructions. DNA libraries were prepared from total RNA using the RNAtag-Seq protocol (78). Briefly, RNA samples were fragmented, depleted of genomic DNA, and dephosphorylated prior to their ligation to barcoded adaptors. Barcoded RNAs were pooled, depleted of rRNA using RiboZero (Epicentre), and converted to Illumina cDNA libraries in 3 steps: (i) reverse transcription of the RNA primed from the ligated adaptor, (ii) degradation of the RNA and ligation of a second adaptor to the single-stranded cDNA, and (iii) PCR amplification of the cDNA with primers targeting the ligated adaptors and carrying the full sequence of the Illumina sequencing adaptors. Libraries were sequenced on HiSeq 2000 to yield 25-base paired-end (PE) reads.

RNA-sequencing data analysis. Sequencing reads were aligned to the H37Rv genome (RefSeq [NC_000962](https://ncbi.nlm.nih.gov/assembly/GCF_000000000.0/)). The overall fragment coverage of genomic regions corresponding to features such as open reading frames and rRNAs based on RefSeq annotations was determined by using bioinformatic pipelines developed in-house as previously described (79). Differential expression analysis was conducted with DESeq (80).

Metabolite extraction and analysis. Metabolite extraction was performed as described previously (81). Briefly, cultures containing $\sim 5 \times 10^8$ bacteria were quenched in 10 ml of 100% methanol at 4°C, spun down, and resuspended in acetonitrile-methanol-water (2:2:1). Cells were lysed mechanically by using a bead beater (MP Biomedicals) and spun down, and metabolites were removed and filtered. Metabolite content was analyzed by UPLC-coupled mass spectrometry (Waters, Manchester, United Kingdom). Column eluents were delivered via electrospray ionization. UPLC was performed in a hydrophilic interaction liquid chromatography-mode gradient elution using an Acquity 1.7- μ m amide column (2.1 by 150 mm) based on a method previously described (82). The flow rate was 0.5 ml/min with mobile phase A (100% acetonitrile) and mobile phase B (100% water), both containing 0.1% formic acid. In both positive and negative modes, the gradient began with 1% B until 1 min, was ramped to 35% B by 14 min and then 60% B by 17 min, was held at 60% B for 1 min, was then ramped to 1% B by 19 min, and was held at 1% B to the end of the run at 20 min. The mass spectrometer was operated in V mode for high sensitivity using a capillary voltage of 2 kV and a cone voltage of 17 V. The desolvation gas flow rate was 500 liters/h, and the source and desolvation gas temperature were 120°C and 325°C, respectively. MS spectra were acquired in centroid mode from m/z 50 to 1,200 with a scan time of 0.5 s. Leucine enkephalin (2 ng/ μ l) was used as lock mass (m/z 556.2771 and 554.2615 in positive and negative experiments, respectively). A TargetLynx (Waters) database was compiled by running standards of metabolites of interest to determine retention times and m/z . All samples were analyzed using TargetLynx (Waters) with manual curation of peak areas where necessary. Peak areas were normalized to number of cells and used to calculate fold changes of metabolites relative to Fe-replete cultures. When peaks were not detected, the peak area was set to 1 to calculate fold changes. Metabolite abundances, retention times, and m/z values can be found in Data Set S2.

Statistical analyses. All experiments were performed in triplicate and repeated on at least two different occasions. Data are expressed as means \pm standard deviations (SD). Differences between frequencies were assessed by Student's *t* test (bilateral and unpaired) using a *P* value of <0.05 as statistically significant. In the microarray analyses, a one-class SAM analysis (83) was performed with the MEV software (84) to find genes with changes that occurred consistently in all replicates. A median false discovery rate (FDR) of zero, delta values ranging from 3.14 to 3.63, and a mean change of at least 2-fold were considered our cutoff for significance. Metabolite analysis was performed using MarkerLynx (Waters) with extended statistic function to identify statistically significant differences of metabolite abundances.

Data availability. The microarray data discussed in this publication have been deposited in NCBI's Gene Expression Omnibus and are accessible through GEO series accession number GSE84554.

SUPPLEMENTAL MATERIAL

Supplemental material for this article may be found at <https://doi.org/10.1128/mBio.01092-17>.

FIG S1, PDF file, 0.1 MB.

FIG S2, PDF file, 0.1 MB.

FIG S3, PDF file, 0.7 MB.

FIG S4, PDF file, 0.1 MB.

FIG S5, PDF file, 0.4 MB.

FIG S6, PDF file, 0.3 MB.

FIG S7, PDF file, 0.03 MB.

TABLE S1, PDF file, 0.2 MB.

DATA SET S1, XLSX file, 0.05 MB.

DATA SET S2, XLSX file, 0.02 MB.

ACKNOWLEDGMENTS

We are very grateful to Issar Smith, David Sherman, and Carl Nathan for sharing mutant *M. tuberculosis* strains and to Erika Shor and Shamba Gupta for assistance with preparing the manuscript.

This work was supported by NIH grants R03AI122069 (to G.M.R.), R21AI119573 (to M.B.), and U19AI107774-04 (to S.M.F. and J.L.). M.J.M. was supported by the South African Medical Research Council and the National Research Foundation. A.S. was supported by T32 AI49928. The funders had no role in study design, data collection and interpretation, or the decision to submit the work for publication.

REFERENCES

- Lillebaek T, Dirksen A, Baess I, Strunge B, Thomsen VØ, Andersen AB. 2002. Molecular evidence of endogenous reactivation of *Mycobacterium tuberculosis* after 33 years of latent infection. *J Infect Dis* 185:401–404. <https://doi.org/10.1086/338342>.
- Mitchison DA. 1985. The action of antituberculosis drugs in short-course chemotherapy. *Tubercle* 66:219–225. [https://doi.org/10.1016/0041-3879\(85\)90040-6](https://doi.org/10.1016/0041-3879(85)90040-6).
- Glaziou P, Sismanidis C, Floyd K, Raviglione M. 2014. Global epidemiology of tuberculosis. *Cold Spring Harb Perspect Med* 5:a017798. <https://doi.org/10.1101/cshperspect.a017798>.
- Rodriguez GM, Neyrolles O. 2014. Metallobiology of tuberculosis. *Microbiol Spectr* 2:MGM2-0012-2013. <https://doi.org/10.1128/microbiolspec.MGM2-0012-2013>.
- Weinberg ED. 1984. Iron withholding: a defense against infection and neoplasia. *Physiol Rev* 64:65–102.
- Reddy PV, Puri RV, Chauhan P, Kar R, Rohilla A, Khera A, Tyagi AK. 2013. Disruption of mycobactin biosynthesis leads to attenuation of *Mycobacterium tuberculosis* for growth and virulence. *J Infect Dis* 208:1255–1265. <https://doi.org/10.1093/infdis/jit250>.
- Wells RM, Jones CM, Xi Z, Speer A, Danilchanka O, Doornbos KS, Sun P, Wu F, Tian C, Niederweis M. 2013. Discovery of a siderophore export system essential for virulence of *Mycobacterium tuberculosis*. *PLoS Pathog* 9:e1003120. <https://doi.org/10.1371/journal.ppat.1003120>.
- Rodriguez GM, Smith I. 2006. Identification of an ABC transporter required for iron acquisition and virulence in *Mycobacterium tuberculosis*. *J Bacteriol* 188:424–430. <https://doi.org/10.1128/JB.188.2.424-430.2006>.
- Pandey R, Rodriguez GM. 2012. A ferritin mutant of *Mycobacterium tuberculosis* is highly susceptible to killing by antibiotics and is unable to establish a chronic infection in mice. *Infect Immun* 80:3650–3659. <https://doi.org/10.1128/IAI.00229-12>.
- Pandey R, Rodriguez GM. 2014. IdeR is required for iron homeostasis and virulence in *Mycobacterium tuberculosis*. *Mol Microbiol* 91:98–109. <https://doi.org/10.1111/mmi.12441>.
- Boelaert JR, Vandecasteele SJ, Appelberg R, Gordeuk VR. 2007. The effect of the host's iron status on tuberculosis. *J Infect Dis* 195:1745–1753. <https://doi.org/10.1086/518040>.
- de Monye C, Karcher DS, Boelaert JT, Gordeuk VR. 1999. Bone marrow macrophage iron grade and survival of HIV-sero positive patients. *AIDS* 13:375–380.
- Gomes MS, Boelaert JR, Appelberg R. 2001. Role of iron in experimental *Mycobacterium avium* infection. *J Clin Virol* 20:117–122. [https://doi.org/10.1016/S1386-6532\(00\)00135-9](https://doi.org/10.1016/S1386-6532(00)00135-9).
- Trousseau A. 1872. Lectures on clinical medicine, p 96. New Sydenham Society, London, United Kingdom.
- Murray MJ, Murray AB, Murray MB, Murray CJ. 1978. The adverse effect of iron depletion on the course of certain infections. *Br Med J* 2:1113–1115. <https://doi.org/10.1136/bmj.2.6145.1113>.
- Ulrichs T, Kosmiadi GA, Trusov V, Jörg S, Pradl L, Titukhina M, Mishenko V, Gushina N, Kaufmann SH. 2004. Human tuberculous granulomas induce peripheral lymphoid follicle-like structures to orchestrate local host defence in the lung. *J Pathol* 204:217–228. <https://doi.org/10.1002/path.1628>.
- Ehlers S, Schaible UE. 2012. The granuloma in tuberculosis: dynamics of a host-pathogen collusion. *Front Immunol* 3:411. <https://doi.org/10.3389/fimmu.2012.00411>.
- Lenaerts A, Barry CE, III, Dartois V. 2015. Heterogeneity in tuberculosis pathology, microenvironments and therapeutic responses. *Immunol Rev* 264:288–307. <https://doi.org/10.1111/imr.12252>.
- Marakalala MJ, Raju RM, Sharma K, Zhang YJ, Eugenin EA, Prideaux B, Daudelin IB, Chen PY, Booty MG, Kim JH, Eum SY, Via LE, Behar SM, Barry CE, III, Mann M, Dartois V, Rubin EJ. 2016. Inflammatory signaling in human tuberculosis granulomas is spatially organized. *Nat Med* 22:531–538. <https://doi.org/10.1038/nm.4073>.
- Schaer DJ, Schaer CA, Buehler PW, Boykins RA, Schoedon G, Alayash AI, Schaffner A. 2006. CD163 is the macrophage scavenger receptor for native and chemically modified hemoglobins in the absence of haptoglobin. *Blood* 107:373–380. <https://doi.org/10.1182/blood-2005-03-1014>.
- Valenti P, Antonini G. 2005. Lactoferrin: an important host defence against microbial and viral attack. *Cell Mol Life Sci* 62:2576–2587. <https://doi.org/10.1007/s00018-005-5372-0>.
- Goetz DH, Holmes MA, Borregaard N, Bluhm ME, Raymond KN, Strong RK. 2002. The neutrophil lipocalin NGAL is a bacteriostatic agent that interferes with siderophore-mediated iron acquisition. *Mol Cell* 10:1033–1043. [https://doi.org/10.1016/S1097-2765\(02\)00708-6](https://doi.org/10.1016/S1097-2765(02)00708-6).
- Saiga H, Nishimura J, Kuwata H, Okuyama M, Matsumoto S, Sato S, Matsumoto M, Akira S, Yoshikai Y, Honda K, Yamamoto M, Takeda K. 2008. Lipocalin 2-dependent inhibition of mycobacterial growth in alveolar epithelium. *J Immunol* 181:8521–8527. <https://doi.org/10.4049/jimmunol.181.12.8521>.
- Corbin BD, Seeley EH, Raab A, Feldmann J, Miller MR, Torres VJ, Ander-

- son KL, Dattilo BM, Dunman PM, Gerads R, Caprioli RM, Nacken W, Chazin WJ, Skaar EP. 2008. Metal chelation and inhibition of bacterial growth in tissue abscesses. *Science* 319:962–965. <https://doi.org/10.1126/science.1152449>.
25. Kehl-Fie TE, Zhang Y, Moore JL, Farrand AJ, Hood MI, Rathi S, Chazin WJ, Caprioli RM, Skaar EP. 2013. MntABC and MntH contribute to systemic *Staphylococcus aureus* infection by competing with calprotectin for nutrient manganese. *Infect Immun* 81:3395–3405. <https://doi.org/10.1128/IAI.00420-13>.
 26. Nakashige TG, Zhang B, Krebs C, Nolan EM. 2015. Human calprotectin is an iron-sequestering host-defense protein. *Nat Chem Biol* 11:765–771. <https://doi.org/10.1038/nchembio.1891>.
 27. Subbian S, Tsenova L, Kim MJ, Wainwright HC, Visser A, Bandyopadhyay N, Bader JS, Karakousis PC, Murrmann GB, Bekker LG, Russell DG, Kaplan G. 2015. Lesion-specific immune response in granulomas of patients with pulmonary tuberculosis: a pilot study. *PLoS One* 10:e0132249. <https://doi.org/10.1371/journal.pone.0132249>.
 28. Timm J, Post FA, Bekker LG, Walther GB, Wainwright CH, Manganelli R, Chan WT, Tsenova L, Gold B, Smith I, Kaplan G, McKinney JD. 2003. Differential expression of iron-, carbon-, and oxygen-responsive mycobacterial genes in the lungs of chronically infected mice and tuberculosis patients. *Proc Natl Acad Sci USA* 100:14321–14326. <https://doi.org/10.1073/pnas.2436197100>.
 29. Rodriguez GM, Gardner R, Kaur N, Phanstiel O. 2008. Utilization of Fe³⁺-acinetoferrin analogs as an iron source by *Mycobacterium tuberculosis*. *Biomaterials* 21:93–103. <https://doi.org/10.1007/s10534-007-9096-5>.
 30. Valway SE, Sanchez MP, Shinnick TF, Orme I, Agerton T, Hoy D, Jones JS, Westmoreland H, Onorato IM. 1998. An outbreak involving extensive transmission of a virulent strain of *Mycobacterium tuberculosis*. *N Engl J Med* 338:633–639. <https://doi.org/10.1056/NEJM199803053381001>.
 31. de Man JC. 1975. The probability of most probable numbers. *Eur J Appl Microbiol* 1:67–78. <https://doi.org/10.1007/BF01880621>.
 32. Ramamurthy T, Ghosh A, Pazhani GP, Shinoda S. 2014. Current perspectives on viable but non-culturable (VBNC) pathogenic bacteria. *Front Public Health* 2:103. <https://doi.org/10.3389/fpubh.2014.00103>.
 33. Gill WP, Hari K, Whiddon MR, Liao RP, Mittler JE, Sherman DR. 2009. A replication clock for *Mycobacterium tuberculosis*. *Nat Med* 15:211–214. <https://doi.org/10.1038/nm.1915>.
 34. Park HD, Guinn KM, Harrell MI, Liao R, Voskuil MI, Tompa M, Schoolnik GK, Sherman DR. 2003. Rv3133c/dosR is a transcription factor that mediates the hypoxic response of *Mycobacterium tuberculosis*. *Mol Microbiol* 48:833–843. <https://doi.org/10.1046/j.1365-2958.2003.03474.x>.
 35. Betts JC, Lukey PT, Robb LC, McAdam RA, Duncan K. 2002. Evaluation of a nutrient starvation model of *Mycobacterium tuberculosis* persistence by gene and protein expression profiling. *Mol Microbiol* 43:717–731. <https://doi.org/10.1046/j.1365-2958.2002.02779.x>.
 36. Voskuil MI. 2004. *Mycobacterium tuberculosis* gene expression during environmental conditions associated with latency. *Tuberculosis* 84: 138–143. <https://doi.org/10.1016/j.tube.2003.12.008>.
 37. Huet G, Daffé M, Saves I. 2005. Identification of the *Mycobacterium tuberculosis* SUF machinery as the exclusive mycobacterial system of [Fe-S] cluster assembly: evidence for its implication in the pathogen's survival. *J Bacteriol* 187:6137–6146. <https://doi.org/10.1128/JB.187.17.6137-6146.2005>.
 38. Merchant SS, Helmann JD. 2012. Elemental economy: microbial strategies for optimizing growth in the face of nutrient limitation. *Adv Microb Physiol* 60:91–210. <https://doi.org/10.1016/B978-0-12-398264-3.00002-4>.
 39. den Hengst CD, Buttner MJ. 2008. Redox control in Actinobacteria. *Biochim Biophys Acta* 1780:1201–1216. <https://doi.org/10.1016/j.bbagen.2008.01.008>.
 40. Chen Z, Hu Y, Cumming BM, Lu P, Feng L, Deng J, Steyn AJ, Chen S. 2016. Mycobacterial WhiB6 differentially regulates ESX-1 and the dos regulon to modulate granuloma formation and virulence in zebrafish. *Cell Rep* 16:2512–2524. <https://doi.org/10.1016/j.celrep.2016.07.080>.
 41. Boshoff H, Xu X, Tahlan K, Dowd CS, Pethe K, Camacho LR, Park TH, Yun CS, Schnappinger D, Ehrt S, Williams KJ, Barry CE, III. 2008. Biosynthesis and recycling of nicotinamide cofactors in *Mycobacterium tuberculosis*. An essential role for NAD in nonreplicating bacilli. *J Biol Chem* 283: 19329–19341. <https://doi.org/10.1074/jbc.M800694200>.
 42. Ramón-García S, Ng C, Jensen PR, Dosanjh M, Burian J, Morris RP, Folcher M, Eltis LD, Grzesiek S, Nguyen L, Thompson CJ. 2013. WhiB7, an Fe-S-dependent transcription factor that activates species-specific repertoires of drug resistance determinants in Actinobacteria. *J Biol Chem* 288:34514–34528. <https://doi.org/10.1074/jbc.M113.516385>.
 43. Giffin MM, Modesti L, Raab RW, Wayne LG, Sohaskey CD. 2012. *ald* of *Mycobacterium tuberculosis* encodes both the alanine dehydrogenase and the putative glycine dehydrogenase. *J Bacteriol* 194:1045–1054. <https://doi.org/10.1128/JB.05914-11>.
 44. McMahon MD, Rush JS, Thomas MG. 2012. Analyses of MbtB, MbtE, and MbtF suggest revisions to the mycobactin biosynthesis pathway in *Mycobacterium tuberculosis*. *J Bacteriol* 194:2809–2818. <https://doi.org/10.1128/JB.00088-12>.
 45. Berg JM, Tymoczko JL, Stryer L. 2002. *Biochemistry*, 5th ed. W. H. Freeman and Company, New York, NY.
 46. Wipperman MF, Sampson NS, Thomas ST. 2014. Pathogen roid rage: cholesterol utilization by *Mycobacterium tuberculosis*. *Crit Rev Biochem Mol Biol* 49:269–293. <https://doi.org/10.3109/10409238.2014.895700>.
 47. Pandey AK, Sassetti CM. 2008. Mycobacterial persistence requires the utilization of host cholesterol. *Proc Natl Acad Sci U S A* 105:4376–4380. <https://doi.org/10.1073/pnas.0711159105>.
 48. Pang X, Vu P, Byrd TF, Ghanny S, Soteropoulos P, Mukamolova GV, Wu S, Samten B, Howard ST. 2007. Evidence for complex interactions of stress-associated regulons in an *mprAB* deletion mutant of *Mycobacterium tuberculosis*. *Microbiology* 153:1229–1242. <https://doi.org/10.1099/mic.0.29281-0>.
 49. Sherman DR, Voskuil M, Schnappinger D, Liao R, Harrell MI, Schoolnik GK. 2001. Regulation of the *Mycobacterium tuberculosis* hypoxic response gene encoding alpha-crystallin. *Proc Natl Acad Sci U S A* 98:7534–7539. <https://doi.org/10.1073/pnas.121172498>.
 50. Voskuil MI, Schnappinger D, Visconti KC, Harrell MI, Dolganov GM, Sherman DR, Schoolnik GK. 2003. Inhibition of respiration by nitric oxide induces a *Mycobacterium tuberculosis* dormancy program. *J Exp Med* 198:705–713. <https://doi.org/10.1084/jem.20030205>.
 51. Olakanmi O, Schlesinger LS, Ahmed A, Britigan BE. 2002. Intraphagosomal *Mycobacterium tuberculosis* acquires iron from both extracellular transferrin and intracellular iron pools: impact of interferon-gamma and hemochromatosis. *J Biol Chem* 277:49727–49734. <https://doi.org/10.1074/jbc.M209768200>.
 52. Sturgill-Koszycki S, Schaible UE, Russell DG. 1996. *Mycobacterium*-containing phagosomes are accessible to early endosomes and reflect a transitional state in normal phagosome biogenesis. *EMBO J* 15:6960–6968.
 53. Wagner D, Maser J, Lai B, Cai Z, Barry CE, III, Höner Zu Bentrup K, Russell DG, Bermudez LE. 2005. Elemental analysis of *Mycobacterium avium*-, *Mycobacterium tuberculosis*-, and *Mycobacterium smegmatis*-containing phagosomes indicates pathogen-induced microenvironments within the host cell's endosomal system. *J Immunol* 174:1491–1500. <https://doi.org/10.4049/jimmunol.174.3.1491>.
 54. Clemens DL, Horwitz MA. 1996. The *Mycobacterium tuberculosis* phagosome interacts with early endosomes and is accessible to exogenously administered transferrin. *J Exp Med* 184:1349–1355. <https://doi.org/10.1084/jem.184.4.1349>.
 55. Lupoli TJ, Fay A, Adura C, Glickman MS, Nathan CF. 2016. Reconstitution of a *Mycobacterium tuberculosis* proteostasis network highlights essential cofactor interactions with chaperone DnaK. *Proc Natl Acad Sci U S A* 113:E7947–E7956. <https://doi.org/10.1073/pnas.1617644113>.
 56. Vaubourgeix J, Lin G, Dhar N, Chenouard N, Jiang X, Botella H, Lupoli T, Mariani O, Yang G, Ouerfelli O, Unser M, Schnappinger D, McKinney J, Nathan C. 2015. Stressed mycobacteria use the chaperone ClpB to sequester irreversibly oxidized proteins asymmetrically within and between cells. *Cell Host Microbe* 17:178–190. <https://doi.org/10.1016/j.chom.2014.12.008>.
 57. Mukamolova GV, Turapov O, Malkin J, Woltmann G, Barer MR. 2010. Resuscitation-promoting factors reveal an occult population of tubercle bacilli in sputum. *Am J Respir Crit Care Med* 181:174–180. <https://doi.org/10.1164/rccm.200905-0661OC>.
 58. McKinney JD, Höner zu Bentrup K, Muñoz-Elias EJ, Miczak A, Chan B, Chan WT, Swenson D, Sacchetti JC, Jacobs WR, Jr, Russell DG. 2000. Persistence of *Mycobacterium tuberculosis* in macrophages and mice requires the glyoxylate shunt enzyme isocitrate lyase. *Nature* 406: 735–738. <https://doi.org/10.1038/35021074>.
 59. Tufariello JM, Chapman JR, Kerantzas CA, Wong KW, Vilchère C, Jones CM, Cole LE, Tinaztepe E, Thompson V, Fenyö D, Niederweis M, Ueberheide B, Phillips JA, Jacobs WR, Jr. 2016. Separable roles for *Mycobacterium tuberculosis* ESX-3 effectors in iron acquisition and virulence. *Proc Natl Acad Sci U S A* 113:E3348–E3357. <https://doi.org/10.1073/pnas.1523321113>.
 60. Marrero J, Rhee KY, Schnappinger D, Pethe K, Ehrt S. 2010. Gluconeogenic carbon flow of tricarboxylic acid cycle intermediates is

- critical for *Mycobacterium tuberculosis* to establish and maintain infection. *Proc Natl Acad Sci U S A* 107:9819–9824. <https://doi.org/10.1073/pnas.1000715107>.
61. Wolff KA, de la Peña AH, Nguyen HT, Pham TH, Amzel LM, Gabelli SB, Nguyen L. 2015. A redox regulatory system critical for mycobacterial survival in macrophages and biofilm development. *PLoS Pathog* 11: e1004839. <https://doi.org/10.1371/journal.ppat.1004839>.
 62. Chouchane S, Giroto S, Kapetanaki S, Schelvis JP, Yu S, Magliozzo RS. 2003. Analysis of heme structural heterogeneity in *Mycobacterium tuberculosis* catalase-peroxidase (KatG). *J Biol Chem* 278:8154–8162. <https://doi.org/10.1074/jbc.M208256200>.
 63. Chouchane S, Lippai I, Magliozzo RS. 2000. Catalase-peroxidase (*Mycobacterium tuberculosis* KatG) catalysis and isoniazid activation. *Biochemistry* 39:9975–9983. <https://doi.org/10.1021/bi0005815>.
 64. Pasca MR, Guglielame P, Arcesi F, Bellinzoni M, De Rossi E, Riccardi G. 2004. Rv2686c-Rv2687c-Rv2688c, an ABC fluoroquinolone efflux pump in *Mycobacterium tuberculosis*. *Antimicrob Agents Chemother* 48: 3175–3178. <https://doi.org/10.1128/AAC.48.8.3175-3178.2004>.
 65. Archibald F. 1983. *Lactobacillus plantarum*, an organism not requiring iron. *FEMS Microbiol Lett* 19:29–32. <https://doi.org/10.1111/j.1574-6968.1983.tb00504.x>.
 66. Wolfe AJ. 2015. Glycolysis for the microbiome generation, p 1–16. *In* Conway T, Cohen PS (ed), *Metabolism and bacterial pathogenesis*. ASM Press, Washington, DC.
 67. Piddington DL, Fang FC, Laessig T, Cooper AM, Orme IM, Buchmeier NA. 2001. Cu,Zn superoxide dismutase of *Mycobacterium tuberculosis* contributes to survival in activated macrophages that are generating an oxidative burst. *Infect Immun* 69:4980–4987. <https://doi.org/10.1128/IAI.69.8.4980-4987.2001>.
 68. Watanabe S, Zimmermann M, Goodwin MB, Sauer U, Barry CE, III, Boshoff HI. 2011. Fumarate reductase activity maintains an energized membrane in anaerobic *Mycobacterium tuberculosis*. *PLoS Pathog* 7:e1002287. <https://doi.org/10.1371/journal.ppat.1002287>.
 69. Hartman T, Weinrick B, Vilchère C, Berney M, Tufariello J, Cook GM, Jacobs WR, Jr. 2014. Succinate dehydrogenase is the regulator of respiration in *Mycobacterium tuberculosis*. *PLoS Pathog* 10:e1004510. <https://doi.org/10.1371/journal.ppat.1004510>.
 70. Geiger R, Rieckmann JC, Wolf T, Basso C, Feng Y, Fuhrer T, Kogadeeva M, Picotti P, Meissner F, Mann M, Zamboni N, Sallusto F, Lanzavecchia A. 2016. L-Arginine modulates T cell metabolism and enhances survival and anti-tumor activity. *Cell* 167:829–842.e13. <https://doi.org/10.1016/j.cell.2016.09.031>.
 71. Keogh D, Tay WH, Ho YY, Dale JL, Chen S, Umashankar S, Williams RB, Chen SL, Dunny GM, Kline KA. 2016. Enterococcal metabolite cues facilitate interspecies niche modulation and polymicrobial infection. *Cell Host Microbe* 20:493–503. <https://doi.org/10.1016/j.chom.2016.09.004>.
 72. Manganelli R, Voskuil MI, Schoolnik GK, Smith I. 2001. The *Mycobacterium tuberculosis* ECF sigma factor sigmaE: role in global gene expression and survival in macrophages. *Mol Microbiol* 41:423–437. <https://doi.org/10.1046/j.1365-2958.2001.02525.x>.
 73. Leong F, Eum S, Via LE, Barry CE, III. 2010. Pathology of tuberculosis in the human lung, p 53–81. *In* Leong FJ, Dartois V, Dick T (ed), *A color atlas of comparative pathology of pulmonary tuberculosis*. CRC Press, Boca Raton, FL.
 74. Cox J, Hein MY, Luber CA, Paron I, Nagaraj N, Mann M. 2014. Accurate proteome-wide label-free quantification by delayed normalization and maximal peptide ratio extraction, termed MaxLFQ. *Mol Cell Proteomics* 13:2513–2526. <https://doi.org/10.1074/mcp.M113.031591>.
 75. Rodriguez GM, Voskuil MI, Gold B, Schoolnik GK, Smith I. 2002. *ideR*, an essential gene in *Mycobacterium tuberculosis*: role of IdeR in iron-dependent gene expression, iron metabolism, and oxidative stress response. *Infect Immun* 70:3371–3381. <https://doi.org/10.1128/IAI.70.7.3371-3381.2002>.
 76. Pandey R, Russo R, Ghanny S, Huang X, Helmann J, Rodriguez GM. 2015. MntR(Rv2788): a transcriptional regulator that controls manganese homeostasis in *Mycobacterium tuberculosis*. *Mol Microbiol* 98:1168–1183. <https://doi.org/10.1111/mmi.13207>.
 77. Dudoit S, Speed TP. 2000. A score test for the linkage analysis of qualitative and quantitative traits based on identity by descent data from sib-pairs. *Biostatistics* 1:1–26. <https://doi.org/10.1093/biostatistics/1.1.1>.
 78. Shishkin AA, Giannoukos G, Kucukural A, Ciulla D, Busby M, Surka C, Chen J, Bhattacharyya RP, Rudy RF, Patel MM, Novod N, Hung DT, Gnrirke A, Garber M, Guttman M, Livny J. 2015. Simultaneous generation of many RNA-seq libraries in a single reaction. *Nat Methods* 12:323–325. <https://doi.org/10.1038/nmeth.3313>.
 79. Mandlik A, Livny J, Robins WP, Ritchie JM, Mekalanos JJ, Waldor MK. 2011. RNA-Seq-based monitoring of infection-linked changes in *Vibrio cholerae* gene expression. *Cell Host Microbe* 10:165–174. <https://doi.org/10.1016/j.chom.2011.07.007>.
 80. Anders S, Huber W. 2010. Differential expression analysis for sequence count data. *Genome Biol* 11:R106. <https://doi.org/10.1186/gb-2010-11-10-r106>.
 81. Berney M, Berney-Meyer L, Wong KW, Chen B, Chen M, Kim J, Wang J, Harris D, Parkhill J, Chan J, Wang F, Jacobs WR, Jr. 2015. Essential roles of methionine and S-adenosylmethionine in the autarkic lifestyle of *Mycobacterium tuberculosis*. *Proc Natl Acad Sci U S A* 112:10008–10013. <https://doi.org/10.1073/pnas.1513033112>.
 82. Paglia G, Hrafnisdóttir S, Magnúsdóttir M, Thorlacius S, Palsson BØ, Thiele I. 2012. Monitoring metabolites consumption and secretion in cultured cells using ultra-performance liquid chromatography quadrupole-time of flight mass spectrometry (UPLC-Q-ToF-MS). *Anal Bioanal Chem* 402:1183–1198. <https://doi.org/10.1007/s00216-011-5556-4>.
 83. Tusher VG, Tibshirani R, Chu G. 2001. Significance analysis of microarrays applied to the ionizing radiation response. *Proc Natl Acad Sci USA* 98:5116–5121. <https://doi.org/10.1073/pnas.091062498>.
 84. Saeed AI, Sharov V, White J, Li J, Liang W, Bhagabati N, Braisted J, Klapa M, Currier T, Thiagarajan M, Sturn A, Snuffin M, Rezantsev A, Popov D, Ryltsov A, Kostukovich E, Borisovskiy I, Liu Z, Vinsavich A, Trush V, Quackenbush J. 2003. TM4: a free, open-source system for microarray data management and analysis. *Biotechniques* 34:374–378.
 85. Fontán PA, Voskuil MI, Gomez M, Tan D, Pardini M, Manganelli R, Fattorini L, Schoolnik GK, Smith I. 2009. The *Mycobacterium tuberculosis* sigma factor sigma B is required for full response to cell envelope stress and hypoxia in vitro, but it is dispensable for in vivo growth. *J Bacteriol* 191:5628–5633. <https://doi.org/10.1128/JB.00510-09>.
 86. de Benoist B, McLean E, Egli I, Cogswell M (ed). 2008. *Worldwide prevalence of anaemia 1993–2005*. WHO Global Database on Anaemia, Geneva, Switzerland. http://www.who.int/nutrition/publications/micronutrients/anaemia_iron_deficiency/9789241596657/en/.